DEPTH DETECTION OF CONDUCTING MARINE MINES VIA EDDY-CURRENT AND CURRENT-CHANNELING RESPONSE

M. Mahmoudi and S. Y. Tan

School of Electrical and Electronic Engineering
Nanyang Technological University
Singapore 639798, Singapore

Abstract—A novel scheme for detecting the location of a metallic mine (modeled as a perfectly conducting sphere and spheroid) in marine environment is presented. This technique takes into account Eddy-Current response (ECR) induced on the conducting marine mines as well as Current-Channeling response (CCR) associated with the perturbation of currents induced in the conductive marine environment. It leverages on the unique electromotive force (EMF) induced in a receiving coil through different orientations of a transmitting coil with respect to the marine mine. Unlike conventional EM sensing apparatus which is used to carry out the measurement at just one attitude at a fixed angle with respect to buried mine, our proposed scheme consists of angular scanning via the symmetry axes of a concentric sensor over the metallic mine in order to obtain a unique normalized induced voltage determining the mine's depth. Simulated results show that this technique has the potential of extending the depth detection range compared with the current method especially in conductive marine environment up to about 2 meters away from the sensor.

1. INTRODUCTION

A considerable amount of unexploded landmines and marine mines over 60 countries threaten the mankind's life [1–3]. To avoid maiming the innocent civilians in the contaminated areas, the eradication of such mines has been investigated by many military organizations and humanitarian agencies around the world while the disposal of marine mines are more arduous and expensive than the mines embedded in

---

Corresponding author: S. Y. Tan (esytan@ntu.edu.sg).

lands [2, 4]. Recently what is more laborious is not just to detect the unexploded ordnances, but to identify and discriminate them. Their identification and discrimination would involve determining the depth, location and orientation of buried mines [5]. Several detection methods such as Ground Penetrating Radar (GPR), metal detector and Electromagnetic Induction (EMI) sensing have been found to explore and discriminate mines in various environments and determine their depth [5–13].

GPR is a well-known method especially for discerning non-metallic landmine in shallow depth based on the dielectric contrast between soil and the mine at the frequency range from 30 MHz to 6 GHz [10], however, it is very sensitive to the soil's moisture, the dielectric contrast between the various intermediate layered medium and the roughness of the surface [11]. The drawbacks of GPR include the large size of its apparatus, complex operation and low sensitivity compared to metal detector [10]. In spite of its penetration depth in dry soil which could be up to 15 m, it has a very low penetration depth of few centimeters in the moist soil and marine environments [12–15]. The generic algorithm with an EM model fusion in microwave X-band demonstrates the complexity of GPR method proposed to estimate the depth through segmenting a suspected region [4].

Recently, many researchers have applied low-frequency EMI sensing to determine the depth of a metallic mine with concentric sensors [1, 5, 16–21]. In [19], it was shown that the eigenvalues of magnetic polarizability tensor can be normalized with respect to the depth of the unexploded ordnance (UXO) by applying a multiplicative scale factor at all frequencies. In this method, it would be necessary to have access to the library eigenvalues derived from unknown object after normalizing for the depth. Another method for the depth up to 2 m was suggested on the basis of simplified analysis in which the depth of an object subjected to a pulsed magnetic field can be determined from the ratio of voltages induced in two receiver coils, irrespective of the object's size [18]. The induced eddy currents for the conducting spheres are used to validate this method [22]. However, the nonlinearity of the mine's depth to the voltage ratio indicates two possible depths, which would be time-consuming to overcome in real-time discrimination [18].

Most of conventional electromagnetic sensing apparatus with concentric sensors carry out the measurements at just one attitude at a fixed angle at top of the surface in which the mine is buried [3, 12]. In fact, the concentric coils which are parallel to the surface of conductive environment have the optimum competence in the measurement of ECR that occurs at the lower depth range. Using such configurations

leads to a considerable inefficiency over the range of depths for which the CCR can exceed the ECR due to the conductivity of background medium [1]. Hence, in our proposed scheme, we have utilized the angular scan to enhance the scattered induced voltage due to the conductivity of the background medium in order to increase the depth detection range.

In this paper, a novel scheme to determine the location and depth of perfectly conducting spherical and spheroidal mines embedded in marine environment is presented. The conductive background medium is assumed to be homogenous with a uniform conductivity σ_s and the object is illuminated with a time-varying electromagnetic fields emanating from the common suitable concentric sensors for underwater applications, e.g., GEM-3 and GEM-5. Through angular scanning we provide a practical approach to measure the CCR especially over the range of depth for which it can exceed the ECR, thus causing an increment in the detection range in the marine environment.

Three different configurations of buried spheroidal mines as the representatives of common deployments of marine mines will be discussed. The uniqueness of the normalized EMF pertaining to the induced voltage in the concentric sensor through angular scanning with respect to the marine mine demonstrates how one can discern the location of both spherical and spheroidal conducting mines at any specific depth.

An analysis of the depth-detection technique of spherical mines through separated-coil system is shown in Section 2, and then the pertinent derivations for spheroidal mines with unified coils are given in Section 3. The effectiveness of this scheme is presented through numerical results in Section 4. Subsequently, the conclusion is given in Section 5.

2. THEORY AND FORMULATION FOR SPHERICAL CONDUCTING OBJECT

Consider a perfectly electric conducting (PEC) sphere as a marine mine embedded in seawater having a uniform conductivity, permeability and permittivity $(\sigma_s, \mu_s, \varepsilon_s)$ as shown in Fig. 1. The transmitting and receiving coils are positioned at the distances of d_t and d_r from the spherical conducting mine of radius a_0, respectively. As depicted, θ_T and θ_R are the angles by which the sphere is displaced from the symmetry dipole axes of the transmitting and receiving coils, respectively. The following assumptions are made to simplify the derivation of EMF induced in the receiving coil:

1 – The transmitting and receiving coils can be approximated as

magnetic dipoles having moments $M_T = N_T A_T I_T$ and $M_R = N_R A_R I_R$, where I_T and I_R are the current in the transmitting and receiving coils, while N_T, N_R, A_T and A_R are the number of turns and the effective areas of transmitting and receiving coils, respectively.

2 – The incident fields H_r^i, H_θ^i and E_ϕ^i emanating from the transmitting coil are uniform over the extent of the object. This assumption is valid as in most cases of d_t and $d_r \gg a_0$.

3 – Sea water is a good conducting medium in such low-frequency range. Thus, displacement current can be neglected. The effect of noise due to the background medium can also be neglected.
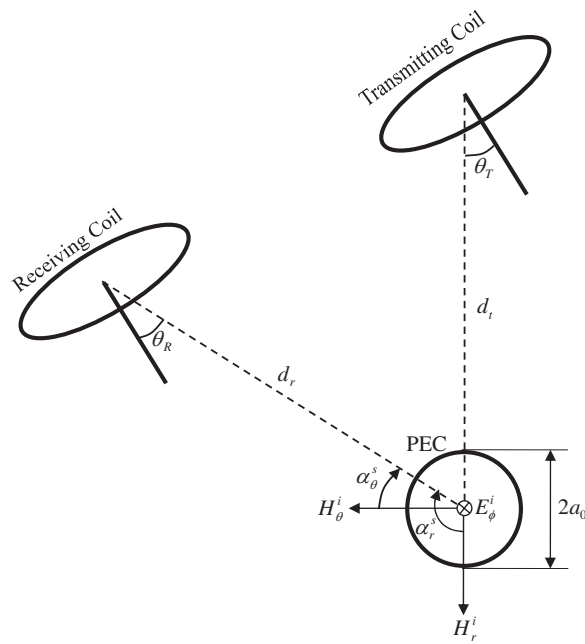

Figure 1. General configuration of mine detection through separate transmitting and receiving coils.

As shown in Fig. 1, the incident fields $\left(H_r^i, H_\theta^i, E_\phi^i \right)$ are given by [21]

$$\overline{H}^i (r_t, \theta_t) = \hat{r}_t H_r^i + \hat{\theta}_t H_\theta^i = \frac{M_T}{4\pi r_t^3} \left(2\hat{r}_t \cos\theta_t + \hat{\theta}_t \sin\theta_t \right) \quad (1a)$$

$$\overline{E}^i (r_t, \theta_t) = \hat{\phi}_t E_\phi^i = \hat{\phi}_t \frac{i\omega\mu_s M_T}{4\pi r_t^2} \sin\theta_t \quad (1b)$$

where $\hat{r}_t, \hat{\theta}_t$ and $\hat{\phi}_t$ are the unit vectors of spherical coordinates defined with the origin at the centre of the transmitting coil and the zenith angle is measured from its surface normal. At the location of the object these electric and magnetic fields are equal to $\overline{H}^i (r_t = d_t, \theta_t = \theta_T)$ and $\overline{E}^i (r_t = d_t, \theta_t = \theta_T)$.

There are two contributions to the EMF (induced voltage) in the receiving coil, namely, the Eddy-Current and Current-Channeling response [12, 21].

2.1. Eddy-Current Response for a Conducting Sphere

For ECR, the current induced in the metallic mine due to the time varying magnetic field is taken into account. The relevant Maxwell's equations can be written as

$$\nabla \times \left(\overline{H}^i + \overline{H}^s \right) = 0, \quad \nabla \cdot \left(\overline{H}^i + \overline{H}^s \right) = 0,$$
$$\nabla \times \left(\overline{E}^i + \overline{E}^s \right) = i\omega\mu_s \left(\overline{H}^i + \overline{H}^s \right) \quad (2)$$

where the time convention of $\exp(-i\omega t)$ is assumed and suppressed throughout. By applying the boundary condition of zero normal component of the magnetic field to the surface of the sphere for each term of the incident magnetic field separately, we can find the total scattered field by

$$\overline{H}_{EC}^s = \overline{H}^s \left(r_s, \alpha_{r,\theta}^s \right) = \overline{H}_r^s (r_s, \alpha_r^s) + \overline{H}_\theta^s (r_s, \alpha_\theta^s) \quad (3)$$

$$\overline{H}_r^s(r_s, \alpha_r^s) = \hat{r}_s H_{r1}^s + \hat{\alpha}_r^s H_{\theta 1}^s = -\frac{M_T a_0^3}{4\pi d_t^3 r_s^3} \cos\theta_T (2\hat{r}_s \cos\alpha_r^s + \hat{\alpha}_r^s \sin\alpha_r^s) (4a)$$

$$\overline{H}_\theta^s(r_s, \alpha_\theta^s) = \hat{r}_s H_{r2}^s + \hat{\alpha}_\theta^s H_{\theta 2}^s = -\frac{M_T a_0^3}{8\pi d_t^3 r_s^3} \sin\theta_T (2\hat{r}_s \cos\alpha_\theta^s + \hat{\alpha}_\theta^s \sin\alpha_\theta^s) (4b)$$

where $\overline{H}_r^s$ and $\overline{H}_\theta^s$ are scattered fields due to the incident fields H_r^i and H_θ^i, respectively.

In Equations (4a) and (4b), the zenith angles α_r^s and α_θ^s are measured from the direction of incident fields H_r^i and H_θ^i at the origin of PEC, respectively. The induced voltage due to the ECR for a receiving coil with moment M_R and current I_R is given by [21]

$$V_{EC}^{sph} = i\omega \frac{M_R}{I_R} \mu_s \overline{H}_{EC}^s \cdot \hat{n} \tag{5}$$

where $\hat{n}$ is the unit vector normal to the receiving coil. The induced voltage due to ECR in the receiving coil shown in Fig. 1 is obtained by

$$V_{EC}^{sph}\left(r_s = d_r, \theta_r = \theta_R\right) = i\frac{N_T N_R A_R A_T I_T a_0^3}{2\pi} \frac{\omega \mu_s}{d_t^3 d_r^3} \bigg(\cos\theta_T \cos\theta_R \cos\alpha_r^s$$

$$+\frac{1}{2}\cos\theta_T\sin\theta_R\sin\alpha_r^s + \frac{1}{2}\sin\theta_T\cos\theta_R\cos\alpha_\theta^s + \frac{1}{4}\sin\theta_T\sin\theta_R\sin\alpha_\theta^s\bigg)(6)$$

2.2. Current-channeling Response for a Conducting Sphere

For CCR, the perturbation of current induced in the sea water (outside of the PEC) is taken into account. The fields obey:

$$\nabla \times \left(\overline{E}^i + \overline{E}^s\right) = 0, \quad \nabla \cdot \left(\overline{E}^i + \overline{E}^s\right) = 0, \quad \nabla \times \widetilde{\overline{H}}^s = \sigma_s \overline{E}^s \tag{7}$$

where $\overline{E}^i$ and $\overline{E}^s$ are the incident and scattered electric fields, respectively. The scattered electric field, $\overline{E}^s$, must have an associated magnetic field defined by $\widetilde{\overline{H}}^s$. By applying the boundary condition of zero tangential component of the electric field on the surface of the sphere, one can obtain the scattered electric field by

$$\overline{E}^s\left(r_s, \alpha_\phi^s\right) = \hat{r}_s E_r^s + \hat{\alpha}_\phi^s E_\theta^s = \frac{i\omega\mu_s M_T a_0^3}{4\pi d_t^2 r_s^3}\sin\theta_T\left(2\hat{r}_s\cos\alpha_\phi^s + \hat{\alpha}_\phi^s\sin\alpha_\phi^s\right) \tag{8a}$$

The corresponding scattered magnetic field can be obtained using (7).

$$\overline{H}_{CC}^s = \widetilde{\overline{H}}^s\left(r_s, \alpha_\phi^s\right) = \hat{\phi}_s \tilde{H}_\phi^s = \hat{\phi}_s \frac{i\omega\mu_s M_T \sigma_s a_0^3}{4\pi d_t^2 r_s^2}\sin\theta_T\sin\alpha_\phi^s \tag{8b}$$

Thus, the induced voltage due to CCR in the receiving coil with moment M_R and current I_R is

$$V_{CC}^{sph}(r_s = d_r, \theta_r = \theta_R) = i\omega\frac{M_R}{I_R}\mu_s\overline{H}_{CC}^s \cdot \hat{n}$$

$$= \frac{N_T N_R A_R A_T I_T a_0^3}{2\pi}\frac{\sigma_s\omega^2\mu_s^2}{2d_t^2 d_r^2}\sin\theta_T\sin\alpha_\phi^s\sin\theta_R \tag{9}$$

where α_ϕ^s and ϕ_s are the zenith and azimuth angles measured by the direction of incident field E_ϕ^i at the origin of PEC, respectively. The total EMF or induced voltage in the receiving coil is equal to

$$V_{tot}^{sph}\left(\alpha_r^s,\alpha_\theta^s,\alpha_\phi^s,\theta_R,\theta_T\right)=V_{EC}^{sph}\left(\alpha_r^s,\alpha_\theta^s,\theta_R,\theta_T\right)+V_{CC}^{sph}\left(\alpha_\phi^s,\theta_R,\theta_T\right) \quad (10)$$

where α_r^s, α_θ^s and α_ϕ^s are determined by the relative configuration of transmitting and receiving coils with respect to each other. On the other hand, θ_T and θ_R are merely dependent upon the position of symmetry axes of transmitting and receiving coils with regards to the conducting object.

3. CONCENTRIC-COIL SYSTEM FOR SPHEROIDAL CONDUCTING OBJECT

The behaviors of scattered fields due to a perfectly conducting prolate spheroidal object, as shown in Fig. 2, are investigated. The major axis of the prolate spheroid is along the z axis while the lengths of the semiminor and semimajor axes are a and b, respectively (with $a > b$). In the prolate spheroidal coordinates (ϑ,ξ,ϕ) by setting $\xi = \xi_0 =$ constant, the surface of a specific spheroid can be defined uniquely in which the length of common interfocal distance, $2D$, is related to the
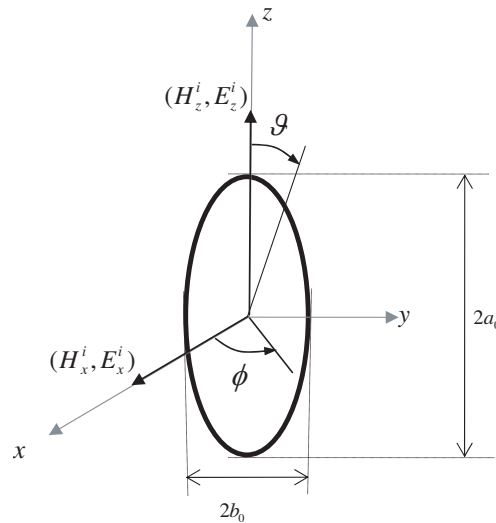

Figure 2. A perfectly conducting prolate spheroidal object being excited with incident electric and magnetic fields.

other parameters in the Cartesian coordinates as follows [23–25],

$$\xi_0 = \frac{a}{D} = \frac{a}{\sqrt{a^2 - b^2}} \tag{11a}$$

$$x = D\sqrt{\xi^2 - 1}\,\sin\vartheta\cos\phi \tag{11b}$$

$$y = D\sqrt{\xi^2 - 1}\,\sin\vartheta\sin\phi \tag{11c}$$

$$z = D\xi\cos\vartheta \tag{11d}$$

where $1 \leq \xi < \infty$, $0 \leq \vartheta \leq \pi$, and $0 \leq \phi \leq 2\pi$. They play the roles of radial coordinate, the colatitude and azimuthal angles in spheroidal coordinates, respectively. The gradient of a scalar function $\psi(\xi, \vartheta, \phi)$ is defined by

$$\nabla\psi = \hat{\xi}\frac{1}{h_\xi}\frac{\partial\psi}{\partial\xi} + \hat{\vartheta}\frac{1}{h_\vartheta}\frac{\partial\psi}{\partial\vartheta} + \hat{\phi}\frac{1}{h_\phi}\frac{\partial\psi}{\partial\phi} \tag{12}$$

where the metrical coefficients are provided by

$$h_\xi = D\frac{\sqrt{\xi^2 - \cos^2\vartheta}}{\sqrt{\xi^2 - 1}} \tag{13a}$$

$$h_\vartheta = D\frac{\sqrt{\xi^2 - \cos^2\vartheta}}{\sin\vartheta} \tag{13b}$$

$$h_\phi = D\sqrt{\xi^2 - 1}\,\sin\vartheta \tag{13c}$$

Here the far-field approximation is the main goal; it can be shown that in the limit as $\xi \to \infty$ one can replace h_ξ, h_ϑ, h_ϕ, $\hat{\xi}$ and $\hat{\vartheta}$ with D, r, $r\sin\theta$, $\hat{r}$ and $\hat{\theta}$ respectively. One can obtain the results for the oblate spheroid directly from those of the prolate spheroid by replacing all ξ_0 with $i\xi_0$ in the prolate formulas given in the following Sections 3.1 and 3.2.

3.1. Eddy-Current Response for a Conducting Prolate Spheroid

Similar to the spherical object, we have all the same assumptions for the uniform incident magnetic field over the extent of the conducting prolate spheroid. According to Fig. 2, the excitation of major and minor axes through the incident magnetic fields, $\overline{H}_z^i$ and $\overline{H}_x^i$, is assumed, respectively. Therefore finding the scattered magnetic fields, $\overline{H}_z^s$ and $\overline{H}_x^s$, for each of the excitations is required in order to compute the induced voltage in any arbitrarily-placed receiving coil pertinent to Eddy-Current response. The incident magnetic fields can be written

as [21]

$$\overline{H}_z^i = H_z^i \hat{z} = -\nabla \psi_z^i, \tag{14a}$$

$$\overline{H}_x^i = H_x^i \hat{x} = -\nabla \psi_x^i \tag{14b}$$

The manipulation of induced potentials $\psi_{z,x}^i$ from Cartesian coordinates into spheroidal ones yields

$$\psi_z^i (\xi, \vartheta) = -H_z^i D\xi \cos \vartheta = -H_z^i D P_1^0(\xi) P_1^0 (\cos \vartheta) \tag{15a}$$

$$\psi_x^i (\xi, \vartheta) = -H_x^i D\sqrt{\xi^2 - 1} \sin \vartheta \cos \phi = -H_x^i D P_1^1(\xi) P_1^1 (\cos \vartheta) \cos\phi \tag{15b}$$

Neglecting any induced currents in the outer space of the spheroid is the essence of Eddy-Current response, while Equation (2) implies that the normal component of magnetic field over the prolate spheroid with infinite conductivity must be zero.

$$\frac{\partial}{\partial \xi} \left[\psi_{z,x}^i + \psi_{z,x}^s \right] \Bigg|_{\xi=\xi_0} = 0 \tag{16}$$

In general, the scattered potential $\psi_{z,x}^s$ can be derived through the series solution containing the first and second kind of Legendre functions as follows

$$\psi_{z,x}^s(\xi, \vartheta, \phi) = \sum_{n=0}^{\infty} \sum_{m=0}^{n} [A_{mn} \cos (m\phi) + B_{mn} \sin (m\phi)] P_n^m (\cos \vartheta) Q_n^m (\xi) \tag{17}$$

The symmetric solution in this problem implies that all m must be zero, then (17) can be reduced to

$$\psi_{z,x}^s = \sum_{n=0}^{\infty} A_n P_n (\cos \vartheta) Q_n(\xi) \tag{18}$$

The orthogonality of the Legendre functions and substituting (15a), (15b) and (18) into (16) give the modified solution for (18) as follows

$$\psi_z^s = A_1 P_1^0 (\cos \vartheta) Q_1^0(\xi) \tag{19a}$$

$$\psi_x^s = A_{11} P_1^1 (\cos \vartheta) Q_1^1(\xi) \cos \phi \tag{19b}$$

Solving the only unknown coefficients A_1 and A_{11}, one can obtain

$$A_1 = H_z^i D \frac{P_1^0 (\xi_0)'}{Q_1^0 (\xi_0)'} \tag{20a}$$

$$A_{11} = H_x^i D \frac{P_1^1 (\xi_0)'}{Q_1^1 (\xi_0)'} \tag{20b}$$

Through computing the gradient of scattered potentials (19a) and (19b), one can obtain the exact solution for the scattered magnetic fields. We apply the large values for the argument of Legendre functions. By using well known properties and approximation of Legendre functions [23] and replacing the metrical coefficients of spheroidal coordinates with the spherical ones as mentioned in Section 3, the scattered magnetic fields are given as follows

$$\overline{H}_z^s(r,\theta) = \frac{H_z^i D^3}{3} \frac{P_1^0(\xi_0)'}{Q_1^0(\xi_0)'} \frac{1}{r^3} \left[2\hat{r}\cos\theta + \hat{\theta}\sin\theta \right] \tag{21a}$$

$$\overline{H}_x^s(r,\theta,\phi) = \frac{2H_x^i D^3}{3} \frac{P_1^1(\xi_0)'}{Q_1^1(\xi_0)'} \frac{1}{r^3}$$
$$\times \left[\hat{r}2\sin\theta\cos\phi - \hat{\theta}\cos\theta\cos\phi + \hat{\phi}\sin\phi \right] \tag{21b}$$

where $\hat{r}$, $\hat{\theta}$ and $\hat{\phi}$ are the unit vectors in spherical coordinates defined with the origin at the centre of prolate spheroid and the zenith angle is measured from the z axis.

3.2. Current-Channeling Response for a Conducting Prolate Spheroid

The geometry of the problem is similar to the Eddy-Current configuration except for the boundary condition which is different for the components of the electric field. The incident electric fields and their pertinent potentials are given as

$$\overline{E}_z^i = E_z^i \hat{z} = -\nabla \psi_z^i \tag{22a}$$

$$\overline{E}_x^i = E_x^i \hat{z} = -\nabla \psi_x^i \tag{22b}$$

The boundary condition on the surface of prolate spheroid with infinite conductivity is a zero tangential component of the electric field as

$$\hat{\xi} \times \nabla \left(\psi_{z,x}^i + \psi_{z,x}^s \right)\Big|_{\xi=\xi_0} = 0 \tag{23}$$

Analogous to the procedure for finding the scattered potential of magnetic fields, one can obtain the scattered potential of electric fields as follows

$$\psi_z^s = E_z^i D \frac{P_1^0(\xi_0)}{Q_1^0(\xi_0)} Q_1^0(\xi) P_1^0(\cos\vartheta) \tag{24a}$$

$$\psi_x^s = E_x^i D \frac{P_1^1(\xi_0)}{Q_1^1(\xi_0)} Q_1^1(\xi) P_1^1(\cos\vartheta) \cos\phi \tag{24b}$$

Subsequently, computing the gradient of scattered potentials of electric fields yields the exact solution as follows

$$\overline{E}_z^s(\xi, \vartheta) = -E_z^i D \frac{P_1^0(\xi_0)}{Q_1^0(\xi_0)} \times \left[\hat{\xi} \frac{Q_1^0(\xi)'}{h_\xi} \cos \vartheta - \hat{\vartheta} \frac{Q_1^0(\xi)}{h_\vartheta} \sin \vartheta \right] \text{(25a)}$$

$$\overline{E}_x^s(\xi, \vartheta, \phi) = -E_x^i D \frac{P_1^1(\xi_0)}{Q_1^1(\xi_0)} \left[\hat{\xi} \frac{Q_1^1(\xi)'}{h_\xi} \sin \vartheta \cos \phi \right.$$
$$\left. + \hat{\vartheta} \frac{Q_1^1(\xi)}{h_\vartheta} \cos \vartheta \cos \phi - \hat{\phi} \frac{Q_1^1(\xi)}{h_\phi} \sin \vartheta \sin \phi \right] \qquad \text{(25b)}$$

Owing to the conductivity of background medium surrounding the prolate spheroid, the scattered electric fields have their associated magnetic fields which must satisfy Equation (7). Therefore using the approximation of Legendre functions [23] and substituting unit vectors with their corresponding ones in spherical coordinates, one can obtain

$$\overline{\tilde{H}}_z^s(r, \theta) = \hat{\phi} \frac{\sigma_0 E_z^i D^3}{3} \frac{P_1^0(\xi_0)}{Q_1^0(\xi_0)} \frac{\sin \theta}{r^2} \qquad \text{(26a)}$$

$$\overline{\tilde{H}}_x^s(r, \theta, \phi) = -\frac{2\sigma_0 E_x^i D^3}{3} \frac{P_1^1(\xi_0)}{Q_1^1(\xi_0)} \frac{1}{r^2} \left[\hat{\theta} \sin \phi + \hat{\phi} \cos \theta \cos \phi \right] \text{(26b)}$$

3.3. Effects of Different Orientations of a Prolate Spheroid on the Induced Voltage

Most of the concealed mines, especially the marine mines, do not have a fixed orientation with regard to the horizontal surface of the area where they are discovered [3]. As it was found in Sections 3.1 and 3.2, the behavior of scattered fields of a spheroidal object is analogous to that of the spherical object in the far field. What causes the induced voltage of a spheroidal mine to be different from a spherical mine pertains to its symmetry axis orientation and the ratio of the semi major axis to its semi minor one. Three representative modes of embedding a spheroidal mine in the conducting medium are considered in Fig. 3. The components of the incident fields used to excite the axes of the spheroid are computed similar to the sphere by Equations (1a) and (1b). Turning the symmetry axis of the transmitting coil on the $x'z'$ plane is a mutual assumption among all the cases and suppressed throughout.
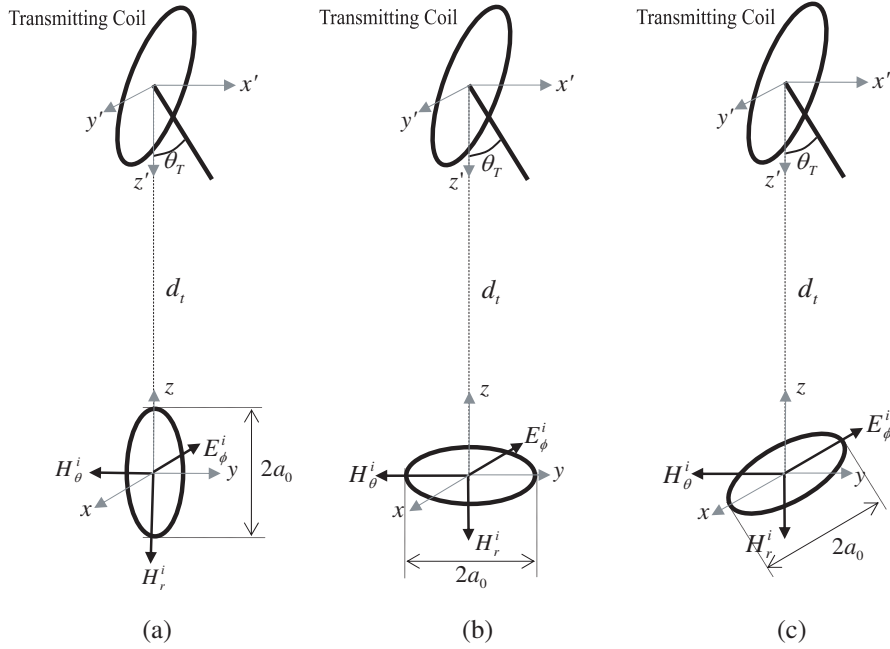
Figure 3. Three representative modes of a spheroidal mine embedded in the conducting medium.

3.3.1. Vertical Prolate Spheroid with Long Axis Perpendicular to the Surface

As shown in Fig. 3(a) the long axis of the prolate spheroid is in the same plane on which the symmetry axis of the receiving coil is laid. Through utilizing the scattering magnetic fields separately for any component of the incident fields, H_r^i, H_θ^i and E_ϕ^i, one can find the induced voltage in the receiving coil corresponding to each element. By applying Equations (21a), (21b) and (5), the ECR due to the incidents magnetic fields, is given by

$$V_{EC}^{pro}(d_t, \xi_0, \theta_T) =$$
$$i\frac{N_T N_R A_T A_R I_T \omega \mu_s D^3}{6\pi d_t^6} \left(\frac{2P_1^0(\xi_0)'}{Q_1^0(\xi_0)'} \cos^2\theta_T + \frac{P_1^1(\xi_0)'}{Q_1^1(\xi_0)'} \sin^2\theta_T \right) \quad (27a)$$

Subsequently, the induced CCR owing to the incident electric field is computed by substituting (26b) into (5).

$$V_{CC}^{pro}(d_t, \xi_0, \theta_T) = \frac{N_T N_R A_T A_R I_T \omega^2 \mu_s^2 \sigma_0 D^3}{6\pi d_t^4} \left(\frac{P_1^1(\xi_0)}{Q_1^1(\xi_0)} \sin^2\theta_T \right) \quad (27b)$$

3.3.2. Horizontal Prolate Spheroid with Long Axis Parallel to Symmetry Axis of the Coil

Figure 3(b) shows how horizontally the prolate spheroid is laid while its long axis is parallel to the symmetry axis of the receiving coil. The displacement of the long axis of the spheroid in this case is what the slight difference in total response towards the vertical spheroid results from. Thus the Eddy-Current response is computed similarly to the vertical mode by using Equations (21a), (21b) and (5).

$$V_{EC}^{pro}\left(d_t, \xi_0, \theta_T\right) =$$
$$i\frac{N_T N_R A_T A_R I_T \omega \mu_s D^3}{12\pi d_t^6}\left(\frac{8P_1^1\left(\xi_0\right)'}{Q_1^1\left(\xi_0\right)'}\cos^2\theta_T + \frac{P_1^0\left(\xi_0\right)'}{Q_1^0\left(\xi_0\right)'}\sin^2\theta_T\right) \quad (28a)$$

The electric field exciting the major axis of the spheroid generates an induced electrical current along the minor axis on the surface of the conducting spheroid. The consequence of the induced current is a perturbation in the surrounding conducting medium. Due to this perturbed current in the medium, the Current-Channeling response is found through utilizing (26b) into (5).

$$V_{CC}^{pro}\left(d_t, \xi_0, \theta_T\right) = \frac{N_T N_R A_T A_R I_T \omega^2 \mu_s^2 \sigma_0 D^3}{6\pi d_t^4}\left(\frac{P_1^1\left(\xi_0\right)}{Q_1^1\left(\xi_0\right)}\sin^2\theta_T\right) \quad (28b)$$

3.3.3. Horizontal Prolate Spheroid with Long Axis Perpendicular to Symmetry Axis of the Coil

The rotation of the previous horizontal conducting spheroid around its minor axis brings about Fig. 3(c) in which the zenith component of the incident magnetic field is aligned along the minor axis of the conducting prolate spheroid. Similar to the vertical spheroid, both major and minor axes are exposed to the incident magnetic fields, thus the ECR in this mode is coming from Equations (21b) and (5) as follows

$$V_{EC}^{pro}\left(d_t, \xi_0, \theta_T\right) =$$
$$i\frac{N_T N_R A_T A_R I_T \omega \mu_s D^3}{6\pi d_t^6}\left(\frac{4P_1^1\left(\xi_0\right)'}{Q_1^1\left(\xi_0\right)'}\cos^2\theta_T + \frac{P_1^1\left(\xi_0\right)'}{Q_1^1\left(\xi_0\right)'}\sin^2\theta_T\right) \quad (29a)$$

The principal distinction between this mode and the two previous ones refers to the direction of the incident electric field which causes a considerable electrical current along the long axis of the conducting prolate spheroid. Owing to the appropriate orientation of the receiving coil with respect to the spheroid, this term can have an essential

effect on the total response. By utilizing Equations (26a) and (5), the Current-Channeling response is given by

$$V_{CC}^{pro}\left(d_t, \xi_0, \theta_T\right) = \frac{N_T N_R A_T A_R I_T \omega^2 \mu_s^2 \sigma_0 D^3}{12 \pi d_t^4} \left(\frac{P_1^0\left(\xi_0\right)}{Q_1^0\left(\xi_0\right)} \sin^2 \theta_T\right) \quad (29\text{b})$$

4. NUMERICAL RESULTS AND DISCUSSION

Consider a GEM-3 sensor [12] in which the transmitting and receiving coils in Fig. 1 are in the same location and orientation with respect to the marine mine. Therefore $\alpha_\theta^s = \alpha_\phi^s = 90°$, $\alpha_r^s = 180°$ and $\theta_T = \theta_R = \theta_0$. A marine mine with $2a_0 = 10\,\text{cm}$ is assumed to be positioned at distance $d_t = d_r = d_0$ from the GEM-3 set at the frequency of $20\,\text{kHz}$. The constitutive parameters of seawater are assumed to be $\mu_s = \mu_0$ and $\sigma_s = 4\,\text{S/m}$ [1]. Fig. 4 shows the angular scan of the normalized total induced voltage in the receiving coil on account of both ECR and CCR, through rotating the angle of symmetry axis of the coils, θ_0, from 0 to 90 degrees with respect to the marine mine positioned at different values of d_0 from the sensor. These angular scans can be used to detect the unknown location of the marine mine.

According to Equations (6) and (9), it is worth noting that the normalized induced voltage in Fig. 4 has a trivial sensitivity to the
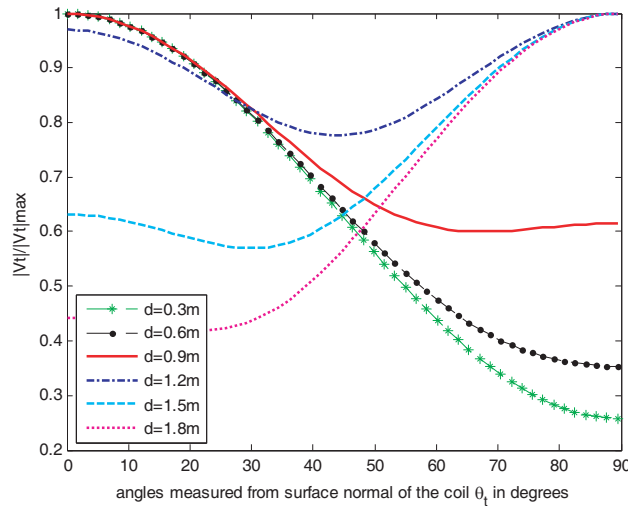

Figure 4. Angular scan of normalized induced voltage for a spherical conducting marine mine at different depths.

size of common marine mines and is appropriate for common metallic spherical mines. After finding the depth of the marine mine by Equations (6) and (9), the absolute induced voltage could provide additional data on the approximate size of the marine mine. Owing to the conductivity of sea water that perturbs the induced currents, higher operating frequencies can amplify the CCR; similarly, through higher distances from the sensor, CCR can substantially exceed ECR.

Figure 4 also depicts that the maximum ECR is obtained when the marine mine is on the symmetry axis of the transmitting coil. On the other hand, the CCR has a zero value on this axis and its maximum occurs at 90° from the symmetry axis. In Sections 3.1 and 3.2, the similarity between the far-field approximations of scattered fields of a conducting spheroidal object and a spherical one demonstrates that applying this methodology for different orientations of a spheroidal mine will lead to obtaining results for a conducting spheroidal mine analogous to Fig. 4. Thus, in order to customize Fig. 4 for a prolate spheroidal object and then utilize it to make a better depth detection, it is merely necessary to investigate the influences of axes aspect ratio, depth and orientation of a conducting spheroidal mine on the induced voltage in the receiving coil relative to a spherical one.

In the following comparison, we assume a conducting spheroidal mine with a major axis equal to the sphere diameter, while the only variable factor is the minor axis of spheroid varying according to its corresponding sphere. Fig. 5(a) depicts how the depth of the buried conducting spheroid shown in Fig. 3(a) with the axes aspect ratio of
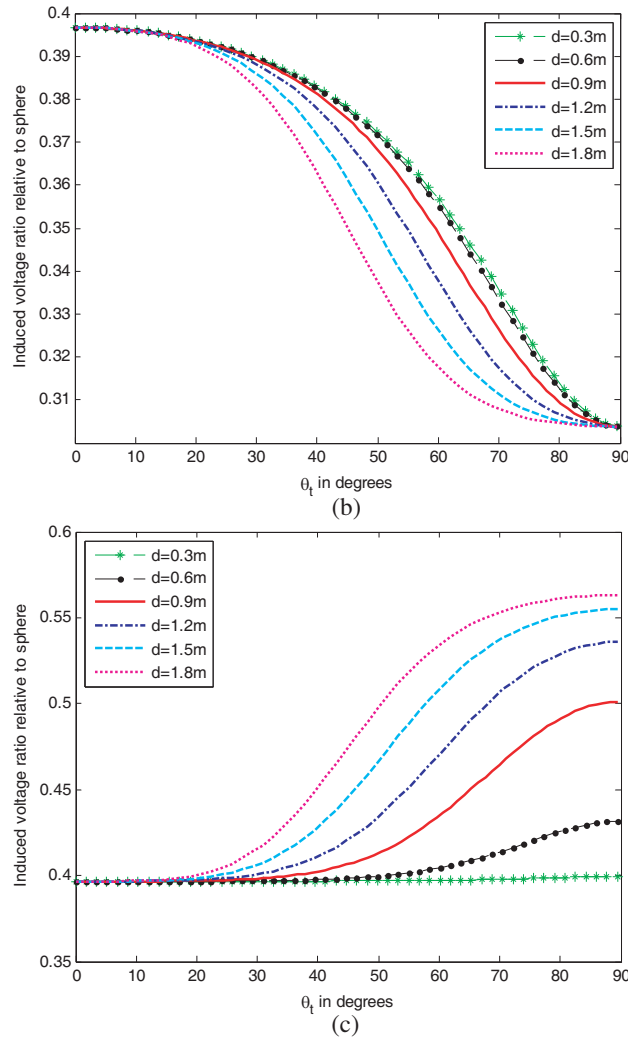

(a)
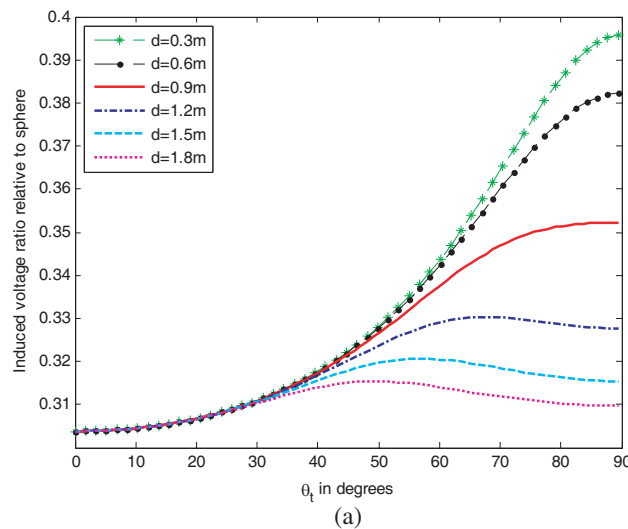
Figure 5. Angular scan of the total induced voltage for a conducting spheroid relative to its corresponding sphere with the axes aspect ratio of 0.6 at different depths for the configuration depicted in (a) Fig. 3(a), (b) Fig. 3(b), (c) Fig. 3(c).

0.6 can affect the total induced voltage in the receiving coil relative to its corresponding sphere at any specific angle. Between the scanning angles of 0 to 40 degrees, all the curves nearly overlay, which indicates that the ECR due to the radial component of incident magnetic field has more influential impact on the total induced voltage than the other

factors. By decreasing the depth of the buried conducting spheroid, one can find its total induced voltage increasing rate against the scanning angle increment regarding the induced voltage due to the corresponding spherical one. It shows that such vertical configuration for a conducting spheroidal mine buried in lower depth has a more sensitive CCR relative to the corresponding one at higher depth. In fact the effect of CCR as applied to the conducting environment can significantly affect the detection range. The absolute value of CCR can dominate the ECR at a higher depth as it has a decay rate proportional to $1/d^4$, while the ECR has a decay rate proportional to $1/d^6$.

It is worth mentioning that when the responses of the conducting spheroids are compared to that of the enclosing spheres, the relative response is always less than 1 as the fundamental consequence of these comparisons. The best interpretation of this behavior is that in the low frequencies applied to the marine mine detection, both spheres and spheroids respond as magnetic dipoles, hence spheres with larger volumes have more effective induced response compared with their corresponding spheroids.

Figures 5(b) and (c) show the results for the two common deploying configurations of spheroidal mines depicted in Fig. 3(b) and Fig. 3(c), respectively. The patterns are observed in Fig. 5(b) and Fig. 5(c) through the increase on the scanning angle from $\theta_0 = 40°$. They can be associated with the angles in which the CCR exceeds the ECR level and this demonstrates that CCR can enhance the discrimination capability in greater depth as well as the ECR does in the lower depth. What is more significant in Fig. 3(c) in comparison to the first two modes is the efficient orientation of the long axis which leads to the higher induced voltage regarding the other configurations. As shown in Fig. 3(c), both radial and zenith components of incident magnetic fields excite the major axis of the spheroid, thus the receiving coil is being excited through a larger part of the spheroid. The effectiveness of CCR is more apparent in Fig. 5(c) in relation to the other modes because the electrical incident field is parallel to the long axis, thus the induced electrical current is provided with the longest path for flowing through the conducting spheroid. To determine the unknown depth of the buried object, the effects of both CCR and ECR are taken into account simultaneously in our scheme. This approach leads to a considerable enhancement up to about 2 m in detection range while the other schemes presented in [12, 21] rely on each of ECR and CCR separately.

Figure 6 shows how the axes aspect ratio of the conducting spheroid depicted in the Fig. 3(a) can affect the induced response in the receiving coil relative to the corresponding sphere at the depth of
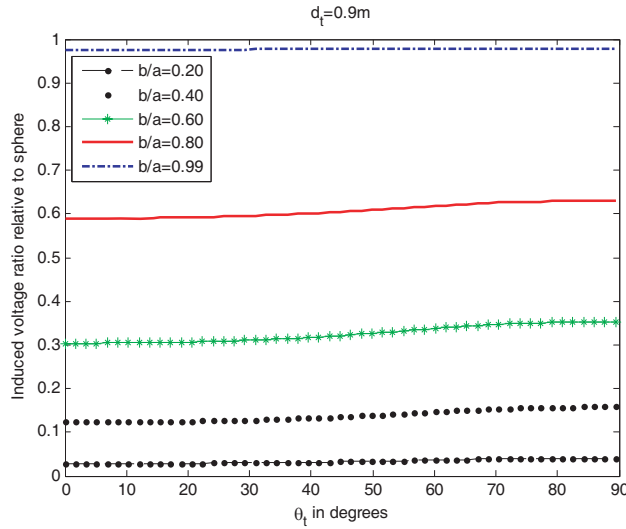
Figure 6. Angular scan of the total induced voltage for a conducting spheroid buried vertically relative to its corresponding sphere with different axes aspect ratio for the depth $d_t = 0.9$ m.

$d_0 = 0.9$ m. By decreasing the aspect ratio b/a towards zero, it is found that the relative response tends towards zero, too. In fact the spheroid stretches into a long thin rod while the aspect ratio b/a tends to zero and consequently the effective surface of the conducting spheroid acting as the scatterer decreases. The spheroid with an axes aspect ratio of $b/a = 0.99$ has the most similar response to its corresponding sphere.

5. CONCLUSION

We have presented a novel scheme which is able to determine the location and depth of a metallic mine embedded in a conducting medium on the foundation of Eddy-Current and Current-Channeling response which can be measured with both separate and concentric transmitting and receiving coils. This technique is based on the uniqueness of the normalized induced voltages measured at different depths through scanning the angle of which the transmitter symmetry axis is displaced from the marine mine. Using some modifications in the normalized graphs through considering the influences of depth, orientation and axes aspect ratio of the spheroid as the fundamental factors, the customized graphs obtained for the conducting spheroidal mines are applicable to variable-depth mine detection as efficiently as

spherical mines. It is found that, in addition to the higher depth which strengthens the magnitude of CCR with respect to the ECR, increasing the scanning angle of the symmetry axis of the coil produces similar results. Furthermore, it is also found that the maximum detection depth in the conducting medium, like coastal seawater or marine environment, can be reached up to about 2 m.

REFERENCES

1. Won, I. J., S. Norton, B. SanFilipo, and F. Funak, "Active broadband electromagnetic detection and classification of buried naval mines," *MTS/IEEE Oceans'02*, Vol. 2, 966–973, Oct. 2002.
2. Wu, R., J. Liu, T. Li, Q. Gao, H. Li, and B. Zhang, "Progress in the research of ground bounce removal for landmine detection with ground penetrating radar," *PIERS Online*, Vol. 1, No. 3, 336–340, 2005.
3. Won, I. J., D. A. Keiswetter, and T. H. Bell, "Electromagnetic induction spectroscopy for clearing landmines," *IEEE Trans. Geoscience and Remote Sensing*, Vol. 39, 703–709, Apr. 2001.
4. Tiwari, K. C., D. Singh, and M. K. Arora, "Development of a model for detection and estimation of depth of shallow buried non-metallic landmine at microwave X-band frequency," *Progress In Electromagnetics Research*, PIER 79, 225–250, 2008.
5. Fernandez, J. P., K. Sun, B. Barrowes, K. O'Neill, I. Shamatava, F. Shubitidze, and K. Paulsen, "Inferring the location of buried UXO using a support vector machine," *Proc. SPIE*, Vol. 6553, Orlando Florida, Apr. 11–12, 2007.
6. Weichman, P. B. and E. M. Lavely, "Study of inverse problems for buried UXO discrimination based on EMI sensor data," *Proceedings of the SPIE*, Vol. 5089, 1189–1200, 2003.
7. Sun, Y., X. Li, and J. Li, "Practical landmine detector using forward-looking ground penetrating radar," *Electronics Letters*, Vol. 41, 97–98, Jan. 2005.
8. Moustafa, K. and K. F. A. Hussein, "Performance evaluation of separated aperture sensor GPR system for land mine detection," *Progress In Electromagnetics Research*, PIER 72, 21–37, 2007.
9. Zainud-Deen, S. H., M. E. Badr, E. El-Deen, K. H. Awadalla, and H. A. Sharshar, "Microstrip antenna with corrugated ground plane surface as a sensor for landmines detection," *Progress In Electromagnetics Research B*, Vol. 2, 259–278, 2008.
10. Sato, M., Y. Hamada, X. Feng, F. Kong, Z. Zeng, and G. Fang,

"GPR using an array antenna for landmine detection," *Near Surface Geophysics*, 3–9, 2004.

11. Nishimoto, M., S. Ueno, and Y. Kimura, "Feature extraction from GPR data for identification of landmine-like objects under rough ground surface," *Journal of Electromagnetic Waves and Applications*, Vol. 20, No. 12, 1577–1586, 2006.

12. SanFilipo, B., S. Norton, and I. J. Won, "The effects of seawater on the EMI response of UXO," *OCEANS, 2005. Proceedings of MTS/IEEE*, Vol. 1, 607–614, 2005.

13. Lindell, I. V. and A. H. Sihvola, "Reflection and transmission of waves at the interface of perfect electromagnetic conductor (PEMC)," *Progress In Electromagnetics Research B*, Vol. 5, 169–183, 2008.

14. Xu, L., Y. C. Guo, and X. W. Shi, "Dielectric half space model for the analysis of scattering from objects on ocean surface," *Journal of Electromagnetic Waves and Applications*, Vol. 21, No. 15, 2287–2296, 2007.

15. Abo-Seida, O. M., "Far-field due to a vertical magnetic dipole in sea," *Journal of Electromagnetic Waves and Applications*, Vol. 20, No. 6, 707–715, 2006.

16. Vafeas, P., G. Perrusson, and D. Lesselier, "Low-frequency solution for a perfectly conducting sphere in a conductive medium with dipolar excitation," *Progress In Electromagnetics Research*, PIER 49, 87–111, 2004.

17. Braunisch, H. H., C. O. Ao, K. O'Neill, and J. A. Kong, "Magnetoquasistatic response of conducting and permeable prolate spheroid under axial excitation," *IEEE Trans. Geoscience and Remote Sensing*, Vol. 39, No. 12, 2689–2701, Dec. 2001.

18. Das, Y., J. E. Mcfee, and R. H. Chesney, "Determination of depth of shallowly buried objects by electromagnetic induction," *IEEE Trans. Geoscience and Remote Sensing*, Vol. 23, 60–66, Jan. 1985.

19. Norton, S. J. and I. J. Won, "Identification of buried unexploded ordnance from broadband electromagnetic induction data," *IEEE Trans. Geoscience and Remote Sensing*, Vol. 39, 2253–2261, Oct. 2001.

20. Ao, C. O., H. Braunisch, K. O'Neill, and J. A. Kong, "Quasi-magnetostatic solution for a conducting and permeable spheroid with arbitrary excitation," *IEEE Trans. Geoscience and Remote Sensing*, Vol. 40, No. 4, 887–897, Apr. 2002.

21. Norton, S. J., W. A. SanFilipo, and I. J. Won, "Eddy-current and current-channeling response to spheroidal anomalies," *IEEE*

Trans. Geoscience and Remote Sensing, Vol. 43, 2200–2209, No. 10, Oct. 2005.

22. Mukerji, S. K., M. George, and M. B. Ramamurthy, "Eddy currents in solid rectangular cores," *Progress In Electromagnetics Research B*, Vol. 7, 117–131, 2008.

23. Abramowitz, M. and I. A. Stegun, *Handbook of Mathematical Functions with Formulas, Graphs, and Mathematical Tables*, Dover, New York, 1965.

24. Kotsis, A. D. and J. A. Roumeliotis, "Electromagnetic scattering by a metallic spheroid using shape perturbation method," *Progress In Electromagnetics Research*, PIER 67, 113–134, 2007.

25. Huang, M. D. and S. Y. Tan, "Efficient electrically small prolate spheroidal antennas coating with a shell of double-negative metamaterials," *Progress In Electromagnetics Research*, PIER 82, 241–255, 2008.